

ORIGINAL ARTICLE

Development of Microstructural and Morphological Cortical Profiles in the Neonatal Brain

Daphna Fenchel^{1,2,3}, Ralica Dimitrova^{2,3,4}, Jakob Seidlitz^{5,6}, Emma C. Robinson⁷, Dafnis Batalle^{2,3,4}, Jana Hutter⁴, Daan Christiaens⁴, Maximilian Pietsch⁴, Jakki Brandon⁴, Emer J. Hughes⁴, Joanna Allsop⁴, Camilla O’Keeffe⁴, Anthony N. Price⁴, Lucilio Cordero-Grande⁴, Andreas Schuh⁸, Antonios Makropoulos⁸, Jonathan Passerat-Palmbach⁸, Jelena Bozek⁹, Daniel Rueckert⁸, Joseph V. Hajnal⁴, Armin Raznahan⁵, Grainne McAlonan^{1,2,3,10}, A. David Edwards^{1,4} and Jonathan O’Muircheartaigh^{1,2,3,4}

¹MRC Centre for Neurodevelopmental Disorders, King’s College London, London, SE1 1UL, UK, ²Sackler Institute for Translational Neurodevelopment, Institute of Psychiatry, Psychology & Neuroscience, King’s College London, London, SE5 8AF, UK, ³Department of Forensic and Neurodevelopmental Sciences, Institute of Psychiatry, Psychology & Neuroscience, King’s College London, London, SE5 8AF, UK, ⁴Department of Perinatal Imaging & Health, School of Biomedical Engineering & Imaging Sciences, Centre for the Developing Brain, King’s College London, London, SE1 7EH, UK, ⁵Developmental Neurogenomics Unit, National Institute of Mental Health, Bethesda, MD 20892, USA, ⁶Department of Psychiatry, University of Cambridge, Cambridge, CB2 0SZ, UK, ⁷Department of Biomedical Engineering, School of Biomedical Engineering & Imaging Sciences, King’s College London, London, SE1 7EU, UK, ⁸Biomedical Image Analysis Group, Department of Computing, Imperial College London, London, SW7 2AZ, UK, ⁹Faculty of Electrical Engineering and Computing, University of Zagreb, Zagreb, 10000, Croatia and ¹⁰South London and Maudsley NHS Foundation Trust, London, SE5 8AZ, UK

Address correspondence to Dr Jonathan O’Muircheartaigh, Forensic and Neurodevelopmental Sciences Department, Institute of Psychiatry, Psychology and Neuroscience, King’s College London, 16 De Crespigny Park, London, SE5 8AF, UK. Email: jonathanom@kcl.ac.uk

Abstract

Interruptions to neurodevelopment during the perinatal period may have long-lasting consequences. However, to be able to investigate deviations in the foundation of proper connectivity and functional circuits, we need a measure of how this architecture evolves in the typically developing brain. To this end, in a cohort of 241 term-born infants, we used magnetic resonance imaging to estimate cortical profiles based on morphometry and microstructure over the perinatal period (37–44 weeks postmenstrual age, PMA). Using the covariance of these profiles as a measure of inter-areal network similarity (morphometric similarity networks; MSN), we clustered these networks into distinct modules. The resulting modules were consistent and symmetric, and corresponded to known functional distinctions, including sensory–motor, limbic, and association regions, and were spatially mapped onto known cytoarchitectonic tissue classes. Posterior regions became more

morphometrically similar with increasing age, while peri-cingulate and medial temporal regions became more dissimilar. Network strength was associated with age: Within-network similarity increased over age suggesting emerging network distinction. These changes in cortical network architecture over an 8-week period are consistent with, and likely underpin, the highly dynamic processes occurring during this critical period. The resulting cortical profiles might provide normative reference to investigate atypical early brain development.

Key words: developing brain, morphometric similarity networks, multimodal MRI, perinatal, structural covariance

Introduction

Brain maturation over the perinatal period is rapid and complex. Although the majority of neurons are at their terminal location, synaptogenesis and myelination are ongoing, and (limited) migration of interneurons continues (Petanjek et al. 2011; Paredes et al. 2016). In the cortex, these processes are coordinated with sensory cortex and pathways developing earliest, prefrontal and association areas later (Flechsig of Leipsic 1901; Huttenlocher 1979). This developing architecture and connectivity is critical for efficient functional signaling, supporting and enabling the later development of cognitive and behavioral abilities.

Although alterations in perinatal neurodevelopmental processes have been associated with later cognitive and behavioral difficulties, quantifying myelo- or cytoarchitecture anatomical circuit development in the living human neonate is challenging. A relatively simple hypothesis of cortical connectivity is “similar prefers similar” (Goulas et al. 2016), meaning areas with similar cytoarchitecture preferentially connect. In this context, magnetic resonance imaging (MRI)-based methods such as regional structural covariance (Evans 2013) offer a proxy measure of brain connectivity, with structural similarity of spatially distinct regions of cortex reflecting coordinated maturation (Alexander-Bloch et al. 2013a). This inter-regional similarity is supported by similar genetic or maturational profiles (Alexander-Bloch et al. 2013b) and transcriptomic profiles (Yee et al. 2018) or associated with changes in disease (e.g., Zuo et al. 2018).

Understanding early structural regional similarity can shed light on how the brain develops into an efficient multifunctional system (Cao et al. 2016) and allows the detection of perturbations in normal development (Di Martino et al. 2014; Morgan et al. 2018). Recent years have seen a rise in studies on brain connectivity networks in the perinatal period (Zhao et al. 2019). Structural covariance networks (SCNs) based on measures of gray matter (GM) volume, cortical thickness (CT), cortical folding, and fiber density in the first 2 years of life have been described (Fan et al. 2011; Nie et al. 2014; Geng et al. 2017). Graph measures of these networks at birth show similar organizational properties to brain networks described in adulthood, suggesting that the nonrandom, efficient architecture of the brain is an inherent characteristic of the system, evident from very early on (Fan et al. 2011; Shi et al. 2012). Moreover, measures derived from GM volume covariance networks were found to differ in neonates with familial risk of schizophrenia (Shi et al. 2012). As different anatomical measures are capturing distinct developmental processes (Rakic 1988) and are controlled by different genetic mechanisms (Panizzon et al. 2009; Chen et al. 2013), different measures of cortical development show specific spatial and temporal patterns in early childhood (Gilmore et al. 2012; Li et al. 2013; Nie et al. 2014; Lyall et al. 2015). Therefore, as might be expected, the resulting single-feature SCNs can be inconsistent.

An alternative approach using multiple anatomical measures to elucidate regional structural similarity has recently been

examined in adolescents and adults (Li et al. 2017; Seidlitz et al. 2018). Compared with SCNs derived from a single technique, this approach allows for the construction of networks for individuals, rather than over a group, enabling the assessment of individual variability masked by group templates or case-control studies (Seghier and Price 2018). The resulting morphometric similarity networks (MSNs) have superior spatial consistency with cortical cytoarchitecture compared with networks based on diffusion imaging or on one structural measure (CT) (Seidlitz et al. 2018). Furthermore, cortical regions shown to be connected (i.e., similar) based on this approach have complementary expression of specific genes (Romero-Garcia et al. 2018; Seidlitz et al. 2018). In adults, these networks are also sensitive to alterations in common (Morgan et al. 2019) and rare (Seidlitz et al. 2019) neurodevelopmental disorders. They also have neurobiological specificity; cortical MSNs differ between patients with genetic syndromes and are aligned with the regional expression of disorder-related genes (Seidlitz et al. 2019). The only work we found to apply MSNs in the perinatal period is a recent study in neonates using a variant of MSNs, where authors were able to successfully predict postmenstrual age (PMA) at scan and differentiated infants born prematurely, with superior performance compared with using single predictive measures (Galdi et al. 2020).

The aim of this work therefore was to examine cortical organization from a multi-morphometric perspective, utilizing MSNs; hypothesizing this approach will provide a more sensitive and informative means to describe the postnatal structure and cytoarchitecture of the brain. We constructed cortical MSNs based on structural/morphological and microstructural diffusion parameters in a sample of 241 infant scanned between 37 and 44 weeks PMA. We hypothesized that, in the period following birth, brain development will be reflected in these networks. Moreover, we were interested in the community structure, or modularity in the neonatal brain, assuming these early clusters will provide the skeleton for developing functionality.

Materials and Methods

Subjects

This work included a sample of neonates participating in the Developing Human Connectome Project (dHCP) (<http://www.developingconnectome.org/>), scanned at the Newborn Imaging Centre at Evelina London Children's Hospital, London, UK. Images are available for download and analysis at the project website. This project has received ethical approval (14/LO/1169, IRAS 138070), and written informed consent was obtained from parents. At the beginning of this specific analysis (October 2018), 383 singleton term-born babies had undergone successfully structural and diffusion acquisitions, reconstruction, and early preprocessing. We next removed 87 subjects who failed the structural or diffusion pipelines as described below or who had missing data (e.g., T1 image). Finally, we removed subjects that

have not passed diffusion QC: 17 subjects at the lower 5% of motion parameters and 46 subjects whose brains moved out of the field of view during scanning, leading to slices missing on the superior surface of the brain. One subject with major basal ganglia lesion was excluded, resulting in a final sample of 241 subjects (born at between 37 and 42 weeks; 128 males) with MR images acquired at PMA 40.92 ± 1.58 weeks (mean \pm sd), range 37.43–44.71 weeks, henceforth “age.” No major brain abnormalities were detected in review of the MRI data by a neonatal neuroradiologist in the subjects included.

Image Acquisition

MR images were acquired on a 3T Philips Achieva scanner without sedation, using a dedicated 32-channel neonatal head coil system (Hughes et al. 2017). Acquisition and reconstruction followed optimized protocols for structural images (Kuklisova-Murgasova et al. 2012; Cordero-Grande et al. 2016, 2018) and multi-shell high angular resolution diffusion imaging (HARDI) (Tournier et al. 2015; Hutter et al. 2018). T2-weighted (T2w) images were obtained using a turbo spin echo (TSE) sequence, acquired in two stacks of 2D slices (in sagittal and axial planes), using parameters: TR=12 s, TE=156 ms, and SENSE factor 2.11 (axial) and 2.58 (sagittal) with overlapping slices (resolution $0.8 \times 0.8 \times 1.6$ mm). T1-weighted (T1w) images were acquired using an IR (inversion recovery) TSE sequence with the same resolution using TR=4.8 s, TE=8.7 ms, and SENSE factor 2.26 (axial) and 2.66 (sagittal). Structural images were reconstructed to a final resolution $0.5 \times 0.5 \times 0.5$ mm, using slice-to-volume registration. Diffusion images were obtained using parameters TR=3800 ms, TE=90 ms, SENSE factor=1.2, multiband factor=4, and resolution $1.5 \times 1.5 \times 3.0$ mm with 1.5 mm slice overlap. Diffusion gradient encoding included images collected at $b=0$ s/mm² (20 repeats), $b=400$ s/mm² (64 directions), $b=1000$ s/mm² (88 directions), and $b=2600$ s/mm² (128 directions), and images were reconstructed to a final resolution of $1.5 \times 1.5 \times 1.5$ mm.

Image Processing

Cortical surface processing and extraction of individual cortical features followed the pipeline described in Makropoulos et al. (2018). Briefly, motion- and bias-corrected T2w images were brain extracted and segmented. White, pial, and midthickness surfaces were extracted, inflated, and projected onto a sphere. This was followed by estimation of cortical features including CT, pial surface area (SA), mean curvature (MC), and a gross proxy of myelin content, defined as the ratio between the T1w and T2w images (Glasser and Van Essen 2011), performed after registering the individual T1 and T2 images together, henceforth “myelin index (MI),” as detailed in Makropoulos et al. (2018). All brains were aligned to the 40-week dHCP surface template (Bozek et al. 2018) using Multimodal Surface Matching (MSM) (Robinson et al. 2013, 2014), run with higher-order regularization constraints (Robinson et al. 2018), to match coarse scale cortical folding (sulcal depth) maps. All other metrics were resampled to the template using this transformation and adaptive barycentric resampling (implemented using Human Connectome Project (HCP) tools, Connectome Workbench (<https://www.humanconnectome.org/software/connectome-workbench>)).

Diffusion images were denoised (Veraart et al. 2016), Gibbs-ringing suppressed (Kellner et al. 2016), and corrected for subject

motion and image distortion with slice-to-volume reconstruction in the multi-shell spherical harmonics and radial decomposition (SHARD) basis (Christiaens et al. 2019a), as described in Christiaens et al. (2019b) and using an image-based field map (Andersson et al. 2003). A tensor model for diffusion data was then fitted using a single shell ($b=1000$), and fractional anisotropy (FA) and mean diffusivity (MD) maps were generated using MRtrix3 (Tournier et al. 2019). Neurite density index (NDI) and orientation dispersion index (ODI) maps were calculated using the NODDI toolbox (Zhang et al. 2012) as previously applied in the neonatal brain (Batalle et al. 2019). We acknowledge that the default parameters used to model NODDI here may not be the optimal for our sample (Guerrero et al. 2019). However, there is currently no agreed standard for infant-specific parameters; therefore we opted for the default to at least permit comparisons with previous literature.

Diffusion maps were registered onto individual T2w images using FSL’s *epi_reg* (FLIRT) (<https://fsl.fmrib.ox.ac.uk>) and then projected onto cortical surface using Connectome Workbench in order to sample imaging features with the same spatial representation. All raw images were visually inspected for motion or image artifact and artifacted data excluded, and processed images were inspected for registration errors.

MSNs Construction

Cortical regions were defined using approximately equal-sized cortical parcellations with Voronoi decomposition at different granularities ($n=50, 100, 150, 200, 250, 300$). This option was chosen over parcellation with a pre-existing atlas in order to minimize the effect of variable regional size when calculating the MSNs. For clarity and presentation, all results shown (other than Supplementary Fig. 1) were based on the $n=150$ parcellation. Network construction followed steps introduced before (Li et al. 2017; Seidlitz et al. 2018): For each subject, each of the eight features was first z-scored across the cortex (to account for feature variation) and then averaged across each ROI in the parcellation, resulting in an eight-feature vector including mean normalized values of CT, MC, MI, SA, FA, MD, NDI, and ODI characterizing each node. Correlation (Pearson’s r) between the eight-feature vectors for every two pairs of regions was calculated using Matlab, resulting in an n regions \times n regions similarity matrix for each subject. A group structural similarity matrix was produced by averaging the 241 individual similarity matrices (Fig. 1), and clustering was performed with affinity propagation. This process was also applied for a “leave-one-out” analysis, where similarity was based on a series of seven-feature vectors, leaving one feature out each time. In addition, typical SCNs for the individual features which are much more common in the literature were also generated by correlating each pair of regions across all subjects, resulting in a group similarity matrix that is based on a single morphometric feature. The values used in this analysis were the raw, un-normalized values.

Association Between MSNs with Age at Scan and Sex

To illustrate the effect of age on the individual morphometric features, Spearman’s correlation (Spearman’s ρ) between the averaged regional single features and age was calculated and results corrected with false discovery rate (FDR) at 5% (Benjamini and Hochberg 1995). Nonparametric correlations were chosen for all age analyses as age at scan was not normally distributed

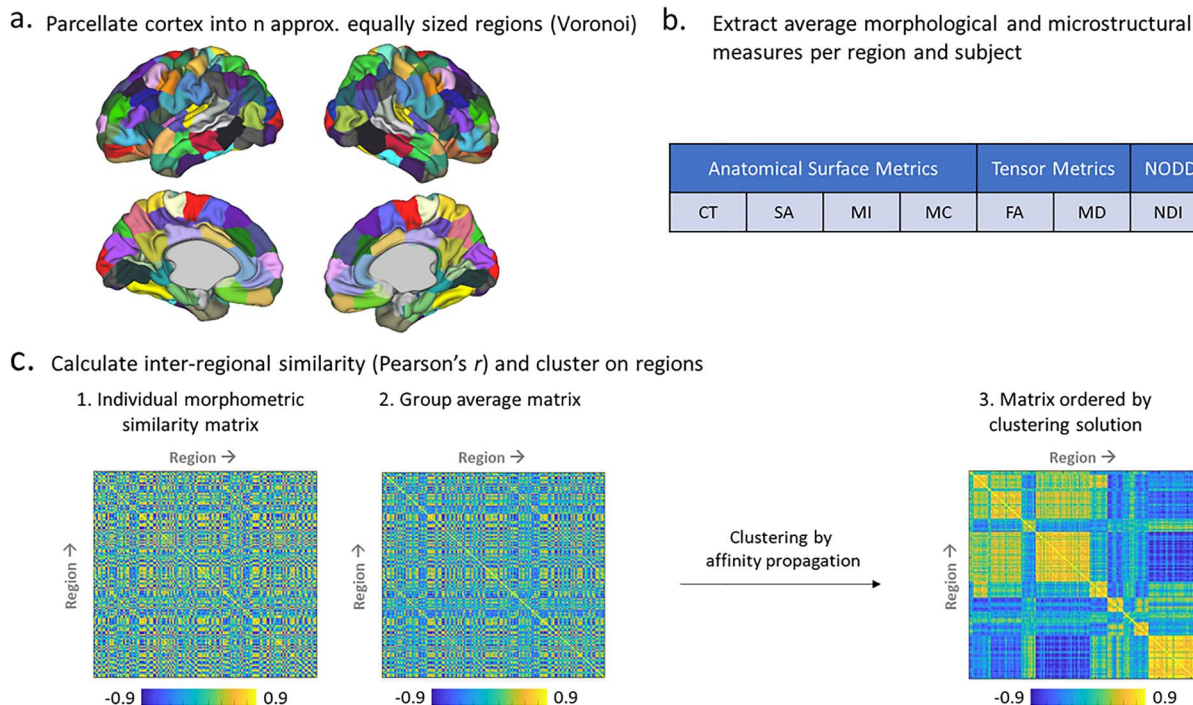


Figure 1. Pipeline for clustering MSNs in the neonatal brain: (a) Cortical regions are defined using Voronoi tessellation of the cortical surface. (b) Each individual region is characterized by an eight-feature vector including averaged normalized values of cortical thickness (CT), mean curvature (MC), myelin index (MI), surface area (SA), fractional anisotropy (FA), mean diffusivity (MD), neurite density index (NDI), and orientation dispersion index (ODI). (c) Each pair of regions is correlated using Pearson's r , resulting in a subject-specific similarity matrix with size n regions \times n regions, which are then averaged to create a group mean similarity matrix, and the resulting group matrix is clustered using affinity propagation algorithm to examine network modularity.

in this sample as indicated by Shapiro–Wilk test ($W(241) = 0.98$, $P = 0.02$).

The effects of age on internodal similarity were examined by correlations between age and the internodal edge-strength. In addition, we investigated the same correlation with *mean* node strength (the *average* of a node's edge-strength with every other node). Sex differences in MSNs for individual edge-strength and mean nodal edge-strength were explored using the Mann–Whitney test. In these contrasts, results were corrected with pFDR (Storey 2002; Storey and Tibshirani 2003), which is advantageous over FDR in larger samples.

MSN Clustering Analysis

To investigate network modularity, the group similarity matrix was clustered using affinity propagation (Frey and Dueck 2007, <https://psi.toronto.edu/?q=tools>). This clustering method has two merits in this current work: First, clustering could be performed without thresholding the group matrix, therefore avoiding information loss due to binarization, and second, it returns the optimal number of clusters (k) for a given preference value. In our case we used the median of the similarity matrix as preference value, making no prior assumptions: While a prespecified k is not mandatory, the algorithm does require an input chosen by the user, termed “preference value.” By choosing the median of the similarity matrix as a shared value, we instruct the algorithm to consider all data points or in our case nodes as “exemplars” for the clusters. In addition, we also performed the same clustering approach but restricted

the solution to a $k = 7$, the number of tissue classes in our von Economo atlas (see below), allowing us to compare this (fixed) clustering solution to clustering solutions from other modalities (see below). The rationale behind $k = 7$ clusters is also based on the maximum rank of the data in the context of a PCA, where the maximum number of components out of eight features from which the MSN was derived (as is the case here) is $k - 1$.

To measure robustness of the MSN clusters to the type of MRI modalities included, and to rank the importance of input modalities to the eventual solution, agreement between the clustering solution for the eight-feature regional vectors and the clustering solutions for seven-feature regional vectors (leave-one-out analysis) and clustering solutions for the eight single features (i.e., SCNs) was examined using normalized variation of information (Meilă 2007; Reichart and Rappoport 2009) using the ‘nvi’ code from the Pattern Recognition and Machine Learning Toolbox for Matlab (<http://prml.github.io/>). As in the leave-one-feature-out analysis, we fixed $k = 7$. In order to rule out the possibility that the clustering solution is derived only from age effects, we also performed clustering on the correlation between the edge-strength and age.

As MSNs in adults have been reported to correspond with cortical cytoarchitecture (Seidlitz et al. 2018), we sought to examine the overlap between the resulting clusters with gross von Economo cytoarchitectural classifications (seven classes) (von Economo and Koskinas 1925) using the Dice coefficient to estimate overlap as in Whitaker et al. (2016). We also attempted to examine the spatial overlap between the seven clusters and von Economo classes using a more rigorous method: spatial

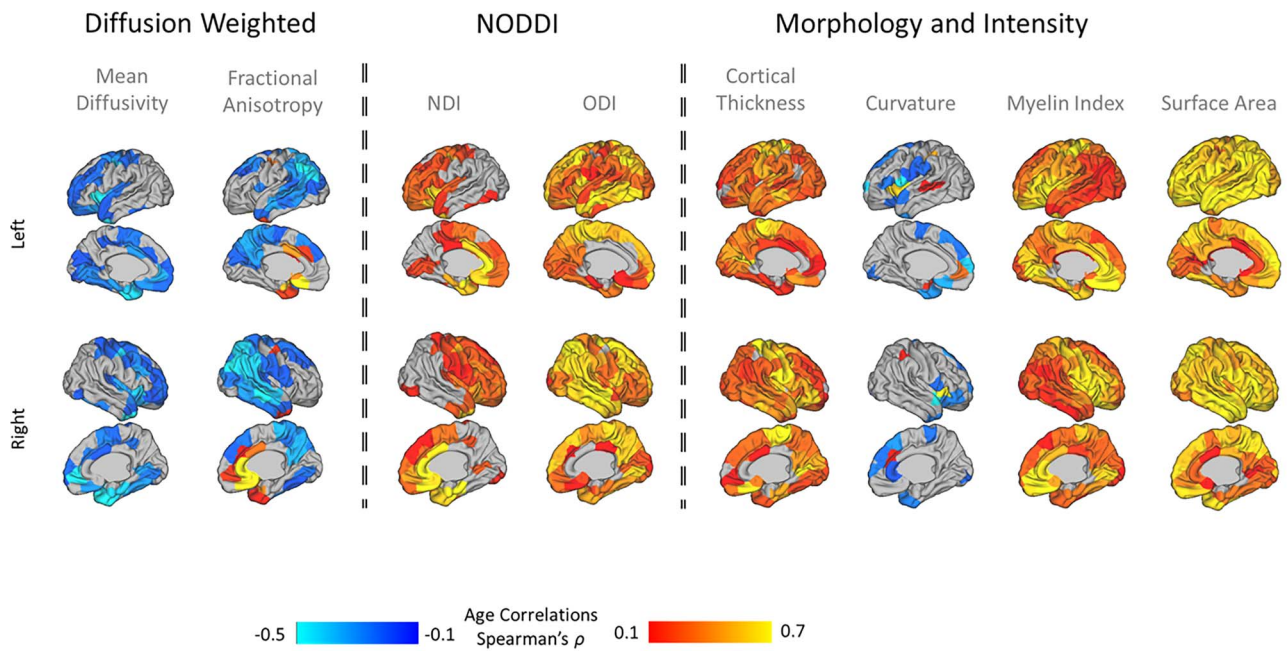


Figure 2. Association between single-feature maps ($n = 150$ parcels) and age at scan: Positive correlations are marked in red and negative correlations in blue. NDI, neurite density index; ODI, orientation dispersion index.

permutations of the spherical representation of the cortical surface (Alexander-Bloch et al. 2018). We generated 500 null distributions for assessing correspondence between the maps as measured by normalized variation of information, while correcting for multiple comparisons as described in Alexander-Bloch et al. (2018).

Association Between MSN Clusters and Age at Scan

To investigate developing network integration and segregation, for each cluster the averaged edge-strength of connections within a cluster (with higher values indicating cluster distinction within the entire network) and the averaged edge-strength of connections between nodes within the cluster and nodes external to that cluster (indicating integration or segregation of that cluster) were calculated. Spearman's ρ coefficients were calculated for changes in these modular integration and segregation measures against age. Results were FDR corrected at 5% (Benjamini and Hochberg 1995).

Results

Age at Scan and Sex Effects

Age-Related Associations with Single-Feature Maps

The correlation between parcellated single-feature maps and age at scan revealed metric-specific age associations: SA and MI had a brain-wide positive association with age, followed by CT, ODI, and NDI that also showed a positive association, but to a lesser extent. FA exhibited both positive and negative associations with age, while MD displayed only a negative association. Significant correlations with MC results were sparser, seen in limited perisylvian, frontal, and temporal regions (Fig. 2). Results are overlaid on a 41-week-old neonatal template (Bozek et al. 2018).

Age- and Sex-Related Associations with MSNs

The correlation between inter-regional edge-strength of MSNs ($n = 150$ parcels) and age at scan showed both positive and negative associations throughout the brain. They numbered less in frontal and anterior temporal regions (see Fig. 3a for a node-by-node count of significant edges). For mean nodal edge-strength, this spatial gradient was clearer, with anterior cingulate and limbic regions negatively associated with age and lateral and medial parietal positively associated (Fig. 3b). Individual edge-strength did show some sex associations (Fig. 3c), though less extensive, with higher edge-strength in lateral frontal and temporal regions in males and cingulum and medial temporal regions in females (Fig. 3d). Age at birth ($U = 6910.5$, $P = 0.55$) and at scan ($U = 6817$, $P = 0.44$) did not differ between males and females.

Modularity of Neonatal MSNs

Using affinity propagation to perform clustering resulted in 12 broadly symmetric cortical modules, aligned with sensory-motor, fronto-temporal, anterior frontal, limbic, cingulate, insular, and visual systems (Fig. 4 left). Comparable spatial findings were also found when the initial parcellation included different number of regions ($n = 50, 100, 150, 200, 250, 300$), but the number of clusters increased linearly with parcellation density. For clarity, results are presented only for the middle density ($n = 150$).

A similar spatial partition was observed when the number of clusters was fixed at seven (Fig. 4 right) and across parcellation densities (Supplementary Fig. 1). The main difference between the 7- and 12-cluster solution was a subdivision of the fronto-temporal and occipital and parietal clusters in the $k = 12$ solution. Therefore, as these changes were minor, with no major loss of information on the overall emerging picture, and as a middle ground between complexity and interpretability, further analyses were performed on the $k = 7$ cluster solution.

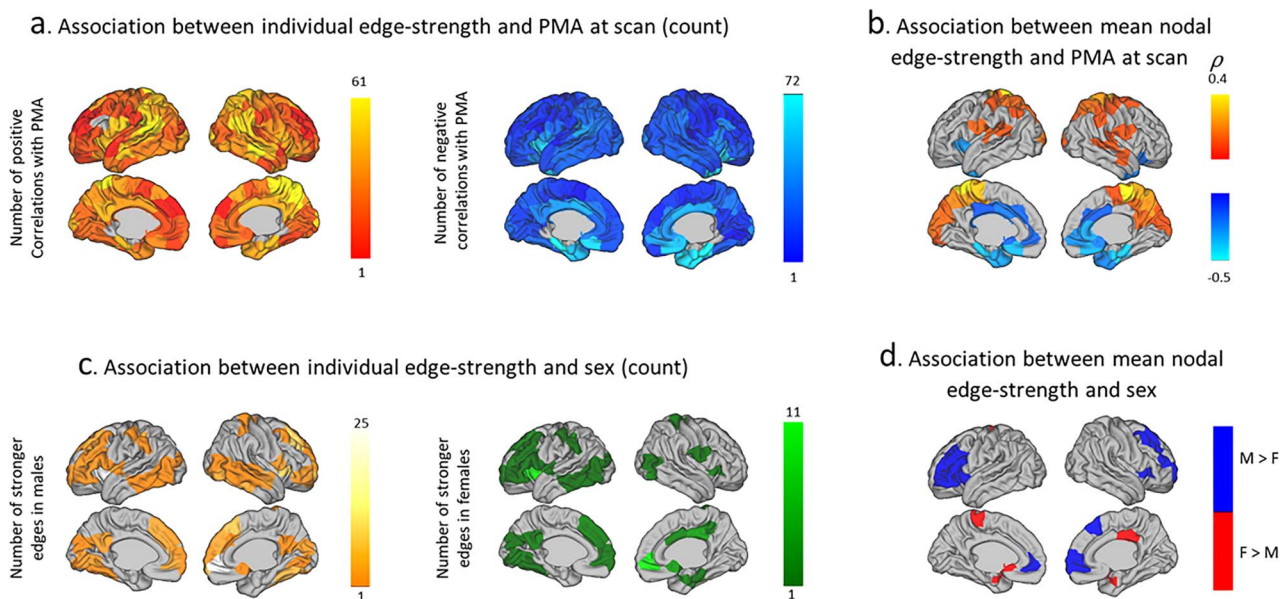


Figure 3. Age and sex associations with MSNs: (a) Sum of positive and negative correlations between internode edge-strength and age at scan. (b) Spearman's correlation between age and mean nodal edge-strength. (c) Sum of stronger internode edges in males (orange) and in females (green). (d) Significant sex differences between mean nodal edge-strength.

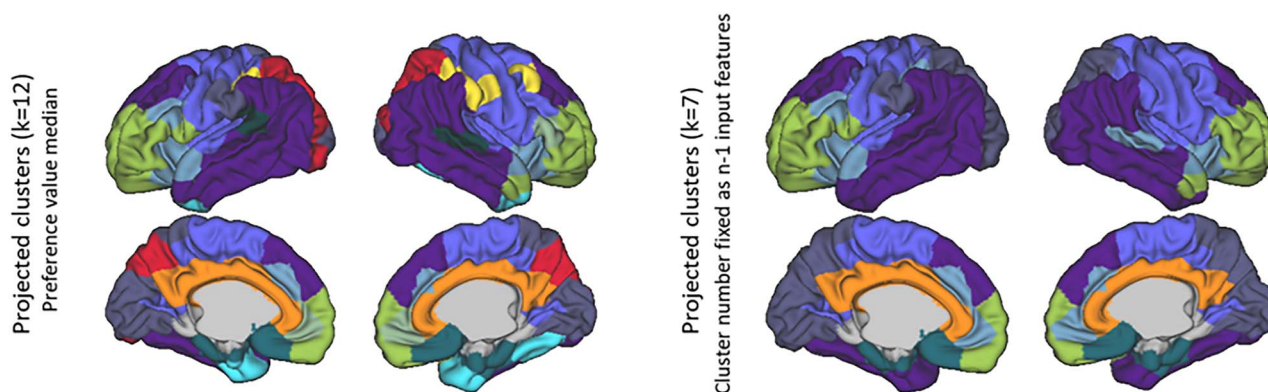


Figure 4. Clustering solution for MSNs created using eight features: Affinity propagation clustering based on a fixed preference value (median similarity) is shown on the left and for a fixed number of clusters on the right.

To confirm the stability of this solution, clustering was calculated using bootstrapping of 20 random subjects each time, for 500 iterations, and individually for each subject. Node coincidence (how often one node fell in the same node as another) was very high (Supplementary Fig. 2b), and even in MSNs of individual infants, the consistency was very good (Supplementary Fig. 2a) with the whole sample cluster structure clearly evident in individuals and bootstrap samples.

Comparing the resulting MSNs (for $k=7$) and von Economo cytoarchitectural classes, similarities were found, more remarkably in limbic and primary sensory areas, as compared with association areas (Fig. 5). Using the spatial permutation test, the normalized variation of information, between the MSN clusters and von Economo classes, was 0.85, ranging $z=0.84-0.93$, suggesting relatively modest overlap; however this overlap was more significant than would be expected by chance ($P=0.02$).

Feature Contribution

Examination of the clustering solution (for $k=7$) for each of the single morphometric measures demonstrated that clustering of FA covariance had the highest agreement with the eight-feature solution (normalized variation of information, $z=0.73$), while clustering of MC covariance had the lowest agreement ($z=0.94$) (Fig. 6a). The top four metrics in particular are strongly correlated with each other cross-sectionally, derived from the same base diffusion-weighted images, and therefore this may indicate redundancy. This pattern remained when the single-feature SCNs were calculated with partial correlation, taking into account age, suggesting this is not exclusively derived by age effects in the individual modalities (data not shown).

In the “leave-one-out” seven-feature solutions, the agreement between modules was much higher than for single modalities, as might be expected. Removing SA and MI from MSN

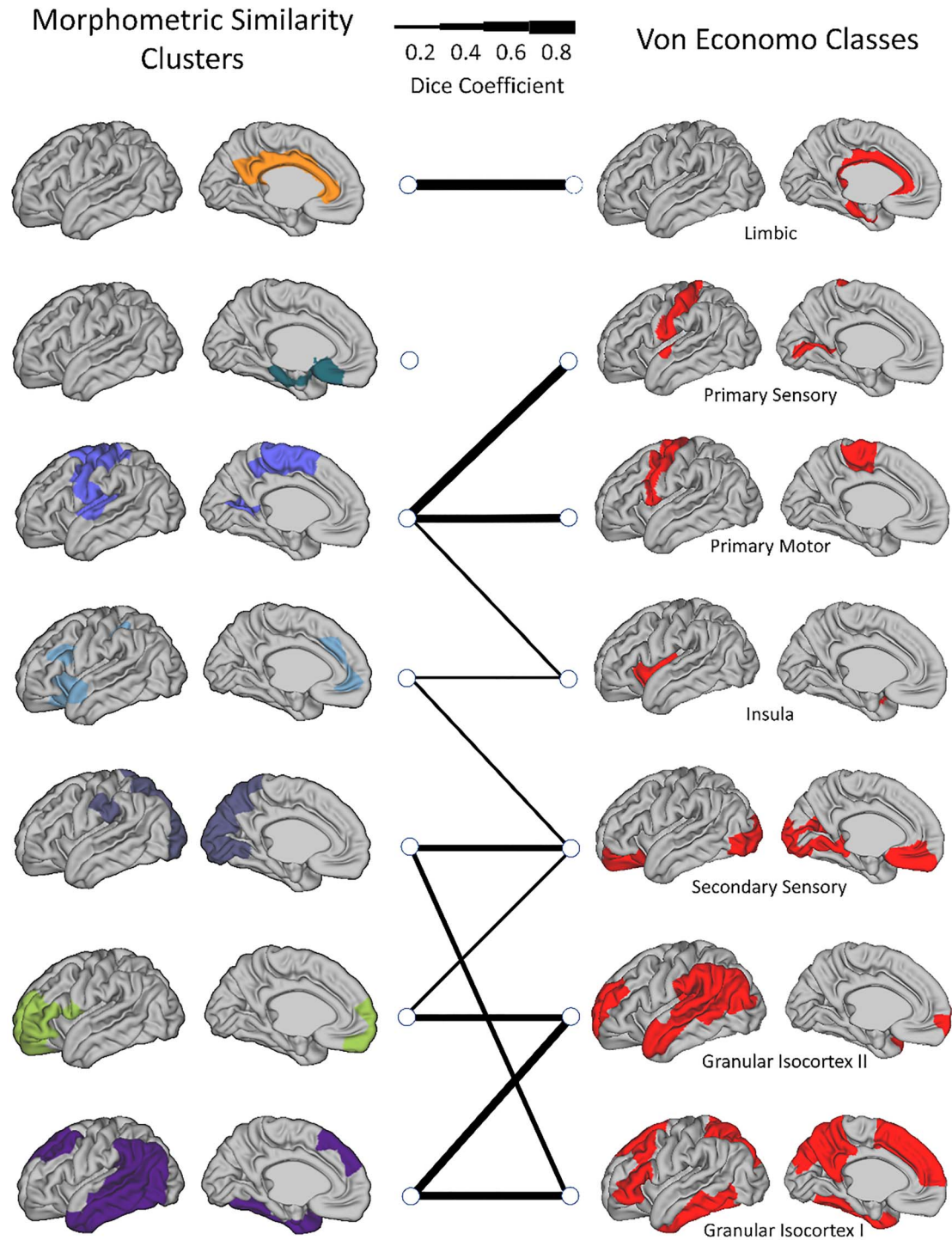


Figure 5. The spatial overlap (Dice coefficients) between MSN clusters and von Economo tissue classes: Line thickness indicates the Dice coefficient per pair of related regions and a Dice of <0.2 is not shown.

estimation had the most profound effect (e.g., resulted in more different clusters), indicating their higher importance to the eventual solution. Removing either MD, NDI, or ODI had less of an effect, with near identical solutions (Fig. 6b).

MSN Clusters and Age at Scan

To demonstrate the age-related changes in cluster differentiation over time, we performed correlations between individual measures of within-module similarity and between-module

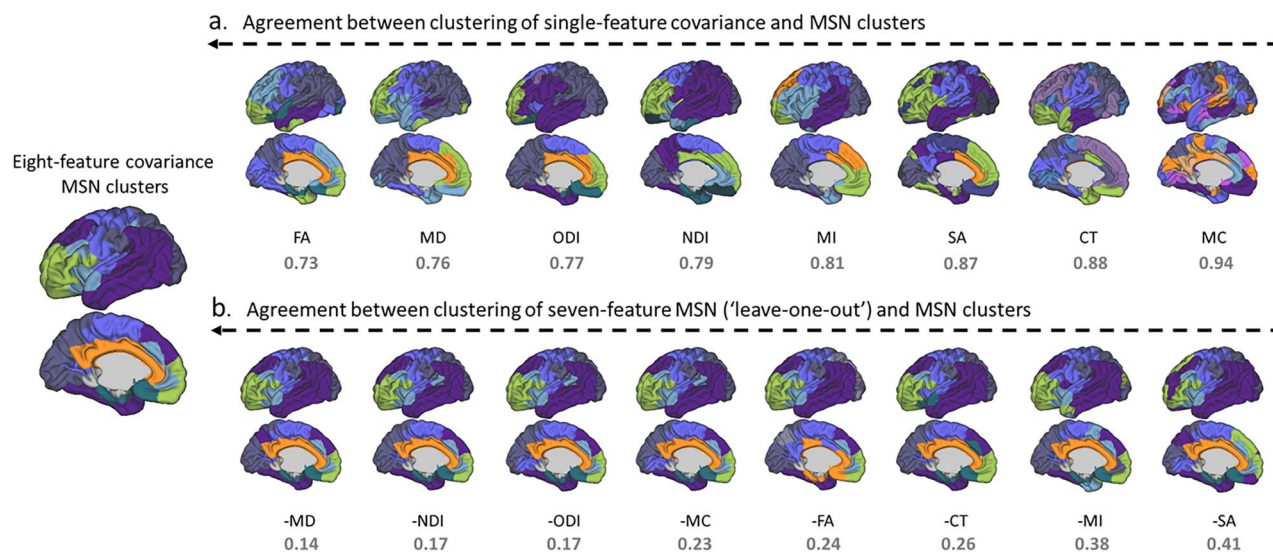


Figure 6. Agreement between clustering solutions using all features with single- and multimeasure covariance: results shown for left hemisphere for ease of interpretation. Clustering solutions are ordered from left (most similar) to right (least similar). (a) Level of agreement between modules derived from a single-feature covariance matrix and the eight-feature MSN. (b) Level of agreement between clustering solution for seven-feature MSN (leave-one-out analysis) and eight-feature MSN. In all cases the normalized variation of information value (z) is shown below (lower is better). CT, cortical thickness; MC, mean curvature; MI, myelin index; SA, surface area; FA, fractional anisotropy; MD, mean diffusivity; NDI, neurite density index; ODI, orientation dispersion index.

similarity. Between-module analysis revealed six cluster pairs with significant positive correlation with age, showing between-cluster integration over time—occipital–parietal and anterior frontal, occipital–parietal and fronto–temporal, limbic and somatosensory–auditory, limbic and cingulate, anterior–frontal and cingulate, and insular–medial frontal and cingulate—while eight cluster pairs showed significant negative correlation with age. The limbic and fronto–temporal clusters demonstrated increased within-module similarity with age, suggesting cluster distinction, or increased internal similarity, while no within-module negative correlation with age was found (Fig. 7). Exact statistical values appear in [Supplementary Table 1](#).

Age-Related Associations with Clustering Solution

Given the clear association between age at scan and connection strength between edges and clusters, we investigated the resulting MSN modules when calculated on edge-by-edge age trajectories. We performed clustering on the correlation matrix of each node-to-node MSN edge against age. This solution demonstrated both a clearly different result ([Supplementary Fig. 3](#)) and also has a different interpretation, showing areas that are similar in their direction and strength of maturation. These results showed more long-range connections and much more heterogeneity in frontal cortex. Primary sensory regions clustered together, and bilateral symmetric fronto–temporal and fronto–parietal networks were also evident.

Discussion

Cortical microstructure and morphology go through extensive changes postnatally. Though the majority of neurons are in situ at term age, myelination and synaptogenesis continue to refine the cortical architecture that will persist throughout the lifespan. Using a densely sampled dataset across the perinatal period, we were able for the first time to combine multiple structural imaging features and showed their utility in exploring

the dynamic progression of brain maturation. We demonstrated a clear and consistent modular structure, with both local and distributed networks of brain regions having similar cortical profiles. This modular structure showed hemispheric symmetry, with correspondence to known long-range cortical functional networks. This structure partly mirrored von Economo classes, indicative of an underlying cellular composition upon which specialized cortical systems will emerge. To our knowledge, this is the first study in neonates using a multiparametric approach to examine the community structure of the neonatal brain.

MSNs are able to capture the extensive changes occurring throughout a short period of just 8 weeks following birth. Age had a complex effect on edge-strength showing both positive and negative correlations, i.e., regional profiles became more and less similar with age. These age associations were confined to occipital, parietal, and temporal areas and were less evident in frontal areas. Whereas these associations were positive (greater morphometric similarity with the rest of the brain), limbic and anterior cingulate regions showed negative correlations with age (less similarity). These findings suggest that in the neonatal period, sensory and limbic areas and posterior parietal regions have the largest maturational changes, as opposed to regions related to higher executive functions (e.g., prefrontal cortex), qualitatively similar to the pattern seen in [Lebenberg et al. \(2019\)](#) with older infants. Changes may only be evident in higher-order areas at a later stage, in line with the more prolonged synaptogenesis, dendritic arborization, and myelination patterns ([Huttenlocher 1990](#); [Huttenlocher and Dabholkar 1997](#); [Teffer and Semendeferi 2012](#)). This may also reflect work in cortical GM volume maturation in neonates, showing a posterior–anterior gradient in the first weeks following birth ([Gilmore et al. 2007](#)). In all, age-dependent changes observed in MSNs in the newborn are in line with neurobiological findings, as well as other neuroimaging findings.

In a mixed sample of term and preterm infants investigating MSNs (derived from structural and extended diffusion metrics,

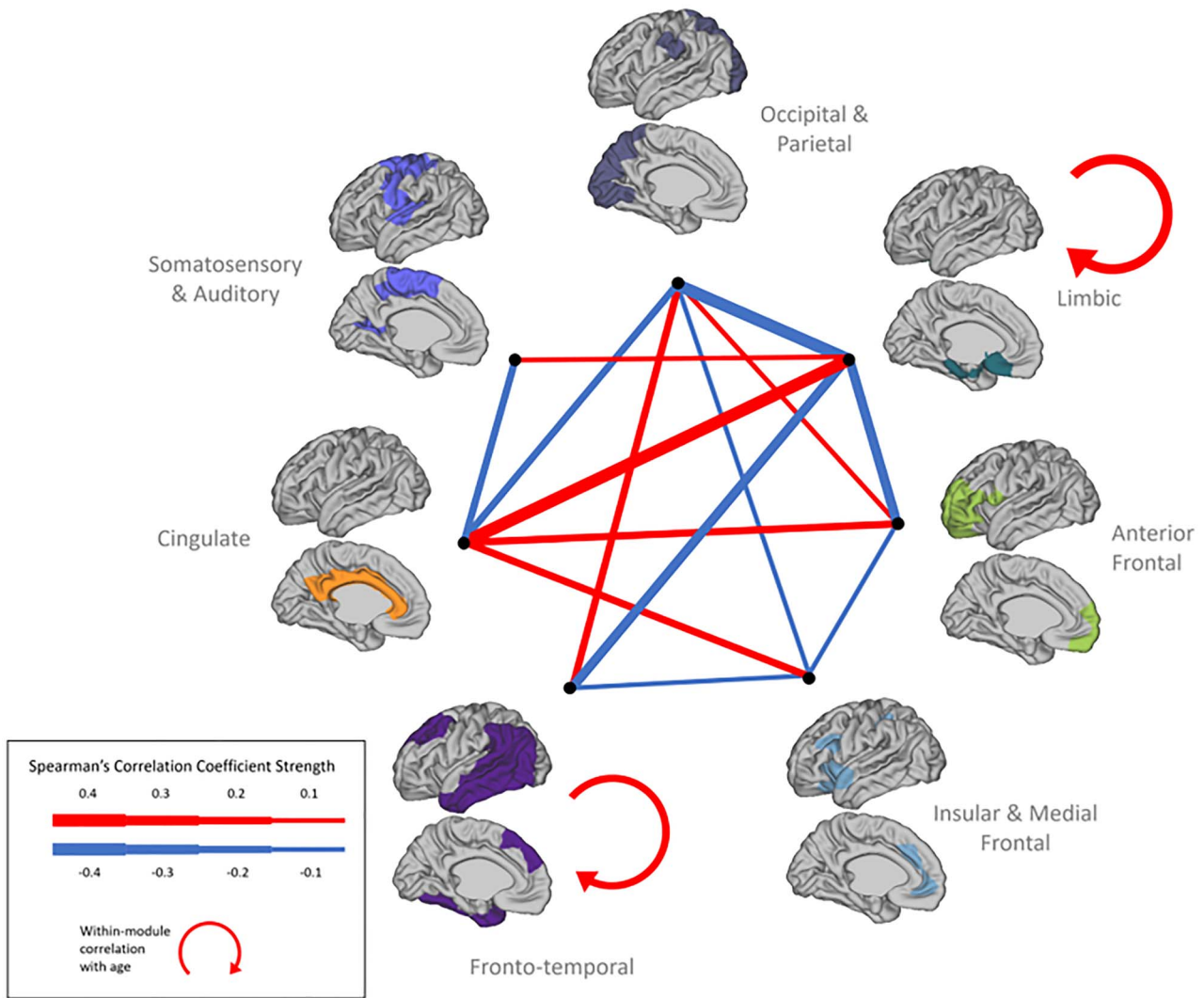


Figure 7. Inter- and intramodular similarity changes with age at scan: association between clusters' edge-strength and age. Width of line is indicative of the strength of significant association.

but not surface measures), Galdi et al. (2020) also found that brain structures became both more similar and dissimilar to each other over the same age range. While that study used different feature vectors, atlas, and populations here, findings are clearly complementary: Occipital connections increased with age, parietal edges were also more positively than negatively associated with age, while temporal edges showed mixed associations with age. In contrast to our findings, frontal regions also showed a strong relationship with age; however, this was more evident in white matter (WM) rather than GM. By choosing to focus only on healthy term-born infants, we attempted to minimize any effects of preterm status confounders on brain maturation (Ball et al. 2017; Batalle et al. 2019).

By exploring the developmental patterns of the individual metrics on which cortical covariance was based, as well as their contribution to the resulting cortical patterning, we were able to dissect early micro and macro properties of the brain. When examining each morphometric measure in isolation, unique developmental trajectories emerged, replicating prior work (Dean et al. 2017; Batalle et al. 2019). However, we also

show that no one measure was able to capture the abundance of unique information that is reflected in the combination of morphometric features. Typical measures of cortical anatomy, thickness, and area, as well as myelin content, showed strong increase with age (Li et al. 2013). Age however showed little significant association with curvature, in agreement with previous reports showing relatively little change in MC compared with other surface measures in the months following birth (Li et al. 2015; Batalle et al. 2019), suggesting that cortical folding remains relatively static in this period. Though no single individual measure mirrored the clustering solution achieved by combining all measures, the diffusion metrics had the better correspondence (Fig. 6a) but were apparently less important to the clustering solution (Fig. 6b). This apparent contradiction is due to redundancy. For example, MD and NDI show very similar patterns of correlation with age (Fig. 2), so removal of one or two diffusion measures does not reduce the effective information used to calculate correlations in MSNs.

Cortical diffusion metrics show complex maturational trajectories around term birth. Ball et al. (2013) and Batalle et al.

(2019) have shown that MD decreases linearly with age, while FA decreases rapidly until week 38 PMA but then begins to slowly increase. This might explain why at the age range examined here (37–44 weeks) we observed both negative and positive associations between FA and age. Moreover, Bataille et al. found that NDI is positively associated with age, similar to the results here. ODI seemed to stabilize after 38 weeks, whereas we still observe a strong association with age after 38 weeks. We might hypothesize that this is related to the focus on preterm neonates in that work, where microstructural trajectories could differ due to earlier birth and the very different early environmental exposures that entail (both clinical and ex utero related).

Sex differences were less widespread compared with age effects. While sex differences in cortical volumes are evident from birth (Gilmore et al. 2007), they are subtle when looking at single modality covariance networks in early development (Zielinski et al. 2010; Geng et al. 2017). Using the MSNs approach, we were able to detect sex effects in some cortical areas, most pronounced in frontal and temporal regions. This corresponds to results of a neonatal study using tensor-based morphometry (Knickmeyer et al. 2014), and even in adults, multimodal imaging sex differences were mainly localized in the frontal lobe, followed by parietal and temporal lobes (Feis et al. 2013), so this may represent a consistent gross pattern throughout the lifespan.

Generally, any network construction and follow-up clustering analyses are highly reliant on several factors, including population and age range examined (Seidlitz et al. 2018; Morgan et al. 2019), type of morphometric measures used (Nie et al. 2013), parcellation (Arslan et al. 2018), threshold (Bordier et al. 2017), wiring cost (Betzel et al. 2017), and type of modularity estimation (Sporns and Betzel 2016) and are therefore likely to vary accordingly. For module definition, we applied affinity propagation to discover meaningful cortical clusters, without eliminating or changing any connections for network construction. In young adults, utilizing MSNs and the Louvain algorithm, Seidlitz et al. (2018) reported four cortical modules consistent with lobular division. Using affinity propagation to cluster similar developing regions in terms of CT and curvedness between the ages 3 and 20 years, Nie et al. (2013) found eight and five clusters, respectively, also with some alignment to lobular division, and indeed our parcellation based just on CT was qualitatively similar.

While most of the resulting modules presented in these studies tend to be spatially contiguous and local, our clustering solution showed also long-range connections and might be more indicative of possible functional and structural connectivity. The modules were broadly aligned with known functional systems and were relatively stable: These included sensory-motor, fronto-parietal, temporal, limbic, cingulate, and visual regions. Our correspondence between MSNs and functional systems may reflect the underlying architecture for later developed functional networks (van den Heuvel et al. 2015; Geng et al. 2017). Our resulting MSN clusters show some overlap to the von Economo tissue classifications, implying the possible origins of the cortical profiles obtained in our analysis, and provide some reassurance of their validity. Further supporting this, the solution revealed here also shows several analogies to the clustering solution of genetic contribution to SA and CT reported by Chen et al. (2013) and might be especially relevant in early development where external environmental effects on these parameters are still relatively small.

The clustering solutions were spatially robust, by and large not affected by age (confirmed by clustering separately only

individuals scanned in the top and bottom PMA-range quartiles), nor was it affected by the neonates' ex utero experience, as the clustering solution for neonates scanned within a week from birth resembled that of the entire sample (data not shown). We also show that the clustering solution is not driven exclusively by age-related changes in the morphometric measures (Supplementary Fig. 3). So, although age did not alter the location of structure of the MSNs, it was associated with their internal coherence. Age was linked to increased regional similarity within the clusters and both increased and decreased regional similarity between clusters (cluster integration and segregation). Though the exact pattern was complex, the summary was that cingulate showed integration with the limbic and insular clusters while segregating from most of the neocortical clusters, perhaps suggesting an advancement towards a more broad representation of paralimbic structures, while the limbic and fronto-temporal clusters showed also age-dependent increase in intrasimilarity.

While our study's advantages include a large neonatal sample, data acquired and analyzed with optimized protocols for this age group, as well as the use of a number of morphometric measures to characterize the brain, it is not without limitations. In order to fully describe development, longitudinal data is needed. Due to the nature of the surface morphometric measures utilized, we were not able to assess whole-brain connectivity, here excluding subcortical structures, cerebellum, and brain stem. Future work should investigate the structural and functional coupling of neonatal MSNs, as well as their genetic and environmental correlates. The implication of recent work using MSNs is that changes in neurodevelopmental disorders must occur early in development. Using a large sample, our study provides a means to detect meaningful alterations in structural coupling at an early stage in infants with either a known genetic or high likelihood to have a later neurodevelopmental disorder.

To conclude, we present cortical MSNs in the neonatal brain, their association with age, and their community structure, characterizing evolving cortical tissue architecture. Following birth, age is strongly related to edge-strength, in a posterior-anterior gradient reflecting the directionality of axonal and dendritic growth, myelination, and synaptogenesis in this period. Clustering of MSNs into modules demonstrated correspondence to known functional systems and cytoarchitectural atlases and was relatively stable across subjects and over the age range examined. Within these clusters, similarity generally seemed to increase postnatally, implying increased network coherence in this short period. We also find a complex relationship of between-clusters similarity, suggesting some rearrangement in segregation and integration of the network, indicative of cortical maturational processes. Here we provide a template of neonatal structural cortical co-variance profiles. By utilizing both shape and microstructural information, we highlight the complex nature of perinatal cortical development.

Supplementary Material

Supplementary material is available at *Cerebral Cortex* online.

Funding

This work was supported by the European Research Council under the European Union Seventh Framework Programme (FP/2007-2013, grant number 319456) for the Developing Human Connectome Project. Infrastructure support was provided by

the National Institute for Health Research (NIHR) Mental Health Biomedical Research Centre at South London, Maudsley NHS Foundation Trust, King's College London and the NIHR Mental Health Biomedical Research Centre at Guy's and St Thomas' Hospitals NHS Foundation Trust. This work was also supported in part by the Wellcome Engineering and Physical Sciences Research Council Centre for Medical Engineering at King's College London (grant number WT 203148/Z/16/Z) and the Medical Research Council (UK) (grant numbers MR/K006355/1, MR/LO11530/1). The views expressed are those of the author(s) and not necessarily those of the NHS, the NIHR or the Department of Health and Social Care. D.F.'s PhD work is supported by the Sackler Institute for Translational Neurodevelopment at King's College London and the Medical Research Council Centre for Neurodevelopmental Disorders, King's College London. J.O.M. is supported by a Sir Henry Dale Fellowship jointly funded by the Wellcome Trust and the Royal Society (grant number 206675/Z/17/Z). J.O.M., D.E. and G.M. received support from the Medical Research Council Centre for Neurodevelopmental Disorders, King's College London (grant number MR/N026063/1).

Notes

We would like to thank the infants and parents who contributed their time to this research. We are also thankful to our colleagues from the Newborn Imaging Centre at Evelina London. *Conflict of Interest.* None declared.

References

- Alexander-Bloch A, Giedd JN, Bullmore E. 2013a. Imaging structural co-variance between human brain regions. *Nat Rev Neurosci.* 14:322–336.
- Alexander-Bloch A, Raznahan A, Bullmore E, Giedd J. 2013b. The convergence of maturational change and structural covariance in human cortical networks. *J Neurosci.* 33:2889–2899.
- Alexander-Bloch AF, Shou H, Liu S, Satterthwaite TD, Glahn DC, Shinohara RT, Vandekar SN, Raznahan A. 2018. On testing for spatial correspondence between maps of human brain structure and function. *Neuroimage.* 178:540–551.
- Andersson JLR, Skare S, Ashburner J. 2003. How to correct susceptibility distortions in spin-echo echo-planar images: application to diffusion tensor imaging. *Neuroimage.* 20:870–888.
- Arslan S, Ktena SI, Makropoulos A, Robinson EC, Rueckert D, Parisot S. 2018. Human brain mapping: a systematic comparison of parcellation methods for the human cerebral cortex. *Neuroimage.* 170:5–30.
- Ball G, Aljabar P, Nongena P, Kennea N, Gonzalez-Cinca N, Falconer S, Chew ATM, Harper N, Wurie J, Rutherford MA et al. 2017. Multimodal image analysis of clinical influences on preterm brain development. *Ann Neurol.* 82:233–246.
- Ball G, Srinivasan L, Aljabar P, Counsell SJ, Durighel G, Hajnal JV, Rutherford MA, Edwards AD. 2013. Development of cortical microstructure in the preterm human brain. *Proc Natl Acad Sci USA.* 110:9541–9546.
- Batalle D, Hughes EJ, Zhang H, Tournier JD, Tusor N, Aljabar P, Wali L, Alexander DC, Hajnal JV, Nosarti C et al. 2017. Early development of structural networks and the impact of prematurity on brain connectivity. *Neuroimage.* 149:379–392.
- Batalle D, O'Muircheartaigh J, Makropoulos A, Kelly CJ, Dimitrova R, Hughes EJ, Hajnal JV, Zhang H, Alexander DC, Edwards AD et al. 2019. Different patterns of cortical maturation before and after 38 weeks gestational age demonstrated by diffusion MRI in vivo. *Neuroimage.* 185:764–775.
- Benjamini Y, Hochberg Y. 1995. Controlling the false discovery rate: a practical and powerful approach to multiple testing. *J R Stat Soc Ser B.* 57:289–300.
- Betzler RF, Medaglia JD, Papadopoulos L, Baum GL, Gur R, Gur R, Roalf D, Satterthwaite TD, Bassett DS. 2017. The modular organization of human anatomical brain networks: accounting for the cost of wiring. *Netw Neurosci.* 1:42–68.
- Bordier C, Nicolini C, Bifone A. 2017. Graph analysis and modularity of brain functional connectivity networks: searching for the optimal threshold. *Front Neurosci.* 11:441.
- Bozek J, Makropoulos A, Schuh A, Fitzgibbon S, Wright R, Glasser MF, Coalson TS, O'Muircheartaigh J, Hutter J, Price AN et al. 2018. Construction of a neonatal cortical surface atlas using multimodal surface matching in the developing human connectome project. *Neuroimage.* 179:11–29.
- Cao M, Huang H, Peng Y, Dong Q, He Y. 2016. Toward developmental connectomics of the human brain. *Front Neuroanat.* 10:25.
- Chen C-H, Fiecas M, Gutiérrez ED, Panizzon MS, Eyler LT, Vuoksimaa E, Thompson WK, Fennema-Notestine C, Hagler DJ, Jernigan TL et al. 2013. Genetic topography of brain morphology. *Proc Natl Acad Sci USA.* 110:17089–17094.
- Christiaens D, Cordero-Grande L, Hutter J, Price AN, Deprez M, Hajnal JV, Tournier J-D. 2019a. Learning compact q-space representations for multi-shell diffusion-weighted MRI. *IEEE Trans Med Imaging.* 38:834–843.
- Christiaens D, Cordero-Grande L, Pietsch M, Hutter J, Price AN, Hughes EJ, Vecchiato K, Deprez M, Edwards AD, Hajnal JV, et al. 2019b. Scattered slice SHARD reconstruction for motion correction in multi-shell diffusion MRI of the neonatal brain. arXiv. 1905.02996.
- Cordero-Grande L, Hughes EJ, Hutter J, Price AN, Hajnal JV. 2018. Three-dimensional motion corrected sensitivity encoding reconstruction for multi-shot multi-slice MRI: application to neonatal brain imaging. *Magn Reson Med.* 79:1365–1376.
- Cordero-Grande L, Teixeira RPAG, Hughes EJ, Hutter J, Price AN, Hajnal JV. 2016. Sensitivity encoding for aligned multishot magnetic resonance reconstruction. *IEEE Trans Comput Imaging.* 2:266–280.
- Dean DC, Planalp EM, Wooten W, Adluru N, Kecskemeti SR, Frye C, Schmidt CK, Schmidt NL, Styner MA, Goldsmith HH et al. 2017. Mapping white matter microstructure in the one month human brain. *Sci Rep.* 7:9759.
- Di Martino A, Fair DA, Kelly C, Satterthwaite TD, Castellanos FX, Thomason ME, Craddock RC, Luna B, Leventhal BL, Zuo X-N et al. 2014. Unraveling the miswired connectome: a developmental perspective. *Neuron.* 83:1335–1353.
- Evans AC. 2013. Networks of anatomical covariance. *Neuroimage.* 80:489–504.
- Fan Y, Shi F, Smith JK, Lin W, Gilmore JH, Shen D. 2011. Brain anatomical networks in early human brain development. *Neuroimage.* 54:1862–1871.
- Feis D-L, Brodersen KH, von Cramon DY, Luders E, Tittgemeyer M. 2013. Decoding gender dimorphism of the human brain using multimodal anatomical and diffusion MRI data. *Neuroimage.* 70:250–257.
- Flechsig of Leipsic P. 1901. Developmental (Myelogenetic) localisation of the cerebral cortex in the human subject. *Lancet.* 158:1027–1030.
- Frey BJ, Dueck D. 2007. Clustering by passing messages between data points. *Science (80-).* 315:972–976.

- Galdi P, Blesa M, Stoye DQ, Sullivan G, Lamb GJ, Quigley AJ, Thrippleton MJ, Bastin ME, Boardman JP. 2020. Neonatal morphometric similarity mapping for predicting brain age and characterizing neuroanatomic variation associated with preterm birth. *NeuroImage Clin.* 102195.
- Geng X, Li G, Lu Z, Gao W, Wang L, Shen D, Zhu H, Gilmore JH. 2017. Structural and maturational covariance in early childhood brain development. *Cereb Cortex.* 27:1795–1807.
- Gilmore JH, Shi F, Woolson SL, Knickmeyer RC, Short SJ, Lin W, Zhu H, Hamer RM, Styner M, Shen D. 2012. Longitudinal development of cortical and subcortical gray matter from birth to 2 years. *Cereb Cortex.* 22:2478–2485.
- Gilmore JH, Lin W, Prastawa MW, Looney CB, Vetsa YSK, Knickmeyer RC, Evans DD, Smith JK, Hamer RM, Lieberman JA et al. 2007. Regional gray matter growth, sexual dimorphism, and cerebral asymmetry in the neonatal brain. *J Neurosci.* 27:1255–1260.
- Glasser MF, Van Essen DC. 2011. Mapping human cortical areas in vivo based on myelin content as revealed by T1- and T2-weighted MRI. *J Neurosci.* 31:11597–11616.
- Goulas A, Werner RR, Beul SF, Saering D, van den Heuvel M, Triarhou LC, Hilgetag CC, Säring D, Van Den Heuvel M, Triarhou LC et al. 2016. Cytoarchitectonic similarity is a wiring principle of the human connectome. *bioRxiv.* 068254.
- Guerrero JM, Adluru N, Bendlin BB, Goldsmith HH, Schaefer SM, Davidson RJ, Kecsckemeti SR, Zhang H, Alexander AL. 2019. Optimizing the intrinsic parallel diffusivity in NODDI: an extensive empirical evaluation. *PLoS One.* 14:e0217118.
- Hughes EJ, Winchman T, Padormo F, Teixeira R, Wurie J, Sharma M, Fox M, Hutter J, Cordero-Grande L, Price AN et al. 2017. A dedicated neonatal brain imaging system. *Magn Reson Med.* 78:794–804.
- Huttenlocher PR. 1979. Synaptic density in human frontal cortex - developmental changes and effects of aging. *Brain Res.* 163:195–205.
- Huttenlocher PR. 1990. Morphometric study of human cerebral cortex development. *Neuropsychologia.* 28:517–527.
- Huttenlocher PR, Dabholkar AS. 1997. Regional differences in synaptogenesis in human cerebral cortex. *J Comp Neurol.* 387:167–178.
- Hutter J, Tournier JD, Price AN, Cordero-Grande L, Hughes EJ, Malik S, Steinweg J, Bastiani M, Sotiropoulos SN, Jbabdi S et al. 2018. Time-efficient and flexible design of optimized multishell HARDI diffusion. *Magn Reson Med.* 79:1276–1292.
- Kellner E, Dhital B, Kiselev VG, Reisert M. 2016. Gibbs-ringing artifact removal based on local subvoxel-shifts. *Magn Reson Med.* 76:1574–1581.
- Knickmeyer RC, Wang J, Zhu H, Geng X, Woolson S, Hamer RM, Konneker T, Styner M, Gilmore JH. 2014. Impact of sex and gonadal steroids on neonatal brain structure. *Cereb Cortex.* 24:2721–2731.
- Kuklisova-Murgasova M, Quaghebeur G, Rutherford MA, Hajnal JV, Schnabel JA. 2012. Reconstruction of fetal brain MRI with intensity matching and complete outlier removal. *Med Image Anal.* 16:1550–1564.
- Lebenberg J, Mangin J-F, Thirion B, Poupon C, Hertz-Pannier L, Leroy F, Adibpour P, Dehaene-Lambertz G, Dubois J. 2019. Mapping the asynchrony of cortical maturation in the infant brain: a MRI multi-parametric clustering approach. *Neuroimage.* 185:641–653.
- Li G, Nie J, Wang L, Shi F, Lin W, Gilmore JH, Shen D. 2013. Mapping region-specific longitudinal cortical surface expansion from birth to 2 years of age. *Cereb Cortex.* 23:2724–2733.
- Li G, Wang L, Shi F, Gilmore JH, Lin W, Shen D. 2015. Construction of 4D high-definition cortical surface atlases of infants: methods and applications. *Med Image Anal.* 25:22–36.
- Li W, Yang C, Shi F, Wu S, Wang Q, Nie Y, Zhang X. 2017. Construction of individual morphological brain networks with multiple morphometric features. *Front Neuroanat.* 11:34.
- Lyall AE, Shi F, Geng X, Woolson S, Li G, Wang L, Hamer RM, Shen D, Gilmore JH. 2015. Dynamic development of regional cortical thickness and surface area in early childhood. *Cereb Cortex.* 25:2204–2212.
- Makropoulos A, Robinson EC, Schuh A, Wright R, Fitzgibbon S, Bozek J, Counsell SJ, Steinweg J, Vecchiato K, Passerat-Palmbach J et al. 2018. The developing human connectome project: a minimal processing pipeline for neonatal cortical surface reconstruction. *Neuroimage.* 173:88–112.
- Meilä M. 2007. Comparing clusterings—an information based distance. *J Multivar Anal.* 98:873–895.
- Morgan SE, White SR, Bullmore ET, Vértes PE. 2018. A network neuroscience approach to typical and atypical brain development. *Biol Psychiatry Cogn Neurosci Neuroimaging.* 3:754–766.
- Morgan SE, Seidlitz J, Whitaker KJ, Romero-Garcia R, Clifton NE, Scarpazza C, van Amelsvoort T, Marcelis M, van Os J, Donohoe G et al. 2019. Cortical patterning of abnormal morphometric similarity in psychosis is associated with brain expression of schizophrenia-related genes. *Proc Natl Acad Sci USA.* 116:9604–9609.
- Nie J, Li G, Shen D. 2013. Development of cortical anatomical properties from early childhood to early adulthood. *Neuroimage.* 76:216–224.
- Nie J, Li G, Wang L, Shi F, Lin W, Gilmore JH, Shen D. 2014. Longitudinal development of cortical thickness, folding, and fiber density networks in the first 2 years of life. *Hum Brain Mapp.* 35:3726–3737.
- Panizzon MS, Fennema-Notestine C, Eyer LT, Jernigan TL, Prom-Wormley E, Neale M, Jacobson K, Lyons MJ, Grant MD, Franz CE et al. 2009. Distinct genetic influences on cortical surface area and cortical thickness. *Cereb Cortex.* 19:2728–2735.
- Paredes MF, James D, Gil-Perotin S, Kim H, Cotter JA, Ng C, Sandoval K, Rowitch DH, Xu D, McQuillen PS et al. 2016. Extensive migration of young neurons into the infant human frontal lobe. *Science (80-).* 354:aaf7073.
- Petanjek Z, Judaš M, Simić G, Rašin MR, Uylings HBM, Rakic P, Kostović I. 2011. Extraordinary neoteny of synaptic spines in the human prefrontal cortex. *Proc Natl Acad Sci USA.* 108:13281–13286.
- Rakic P. 1988. Specification of cerebral cortical areas. *Science.* 241:170–176.
- Reichart R, Rappoport A. 2009. The NVI clustering evaluation measure. In: *Proceedings of the Thirteenth Conference on Computational Natural Language Learning*, 165–173.
- Robinson EC, Garcia K, Glasser MF, Chen Z, Coalson TS, Makropoulos A, Bozek J, Wright R, Schuh A, Webster M et al. 2018. Multimodal surface matching with higher-order smoothness constraints. *Neuroimage.* 167:453–465.
- Robinson EC, Jbabdi S, Andersson J, Smith S, Glasser MF, Van Essen DC, Burgess G, Harms MP, Barch DM, Jenkinson M. 2013. Multimodal surface matching: Fast and generalisable cortical registration using discrete optimisation. In: Gee JC, Joshi S, Pohl KM, Wells WMZL, editors. *Information processing in medical imaging. Lecture notes in computer science.* Berlin, Heidelberg: Springer, pp. 475–486.

- Robinson EC, Jbabdi S, Glasser MF, Andersson J, Burgess GC, Harms MP, Smith SM, Van Essen DC, Jenkinson M. 2014. MSM: a new flexible framework for multimodal surface matching. *Neuroimage*. 100:414–426.
- Romero-Garcia R, Whitaker KJ, Váša F, Seidlitz J, Shinn M, Fonagy P, Dolan RJ, Jones PB, Goodyer IM, Bullmore ET et al. 2018. Structural covariance networks are coupled to expression of genes enriched in supragranular layers of the human cortex. *Neuroimage*. 171:256–267.
- Seghier ML, Price CJ. 2018. Interpreting and utilising intersubject variability in brain function. *Trends Cogn Sci*. 22:517–530.
- Seidlitz J, Váša F, Shinn M, Romero-Garcia R, Whitaker KJ, Vértes PE, Wagstyl K, Kirkpatrick Reardon P, Clasen L et al. 2018. Morphometric similarity networks detect microscale cortical organization and predict inter-individual cognitive variation. *Neuron*. 97:231–247.e7.
- Seidlitz J, Nadig A, Liu S, Bethlehem RAI, Vértes PE, Morgan SE, Váša F, Romero-Garcia R, Lalonde FM, Clasen LS et al. 2019. Transcriptomic and cellular decoding of regional brain vulnerability to neurodevelopmental disorders. *bioRxiv*. 573279.
- Shi F, Yap PT, Gao W, Lin W, Gilmore JH, Shen D. 2012. Altered structural connectivity in neonates at genetic risk for schizophrenia: a combined study using morphological and white matter networks. *Neuroimage*. 62:1622–1633.
- Sporns O, Betzel RF. 2016. Modular brain networks. *Annu Rev Psychol*. 67:613–640.
- Storey JD. 2002. A direct approach to false discovery rates. *J R Stat Soc Ser B (Statistical Methodol)*. 64:479–498.
- Storey JD, Tibshirani R. 2003. Statistical significance for genome-wide studies. *Proc Natl Acad Sci USA*. 100:9440–9445.
- Teffer K, Semendeferi K. 2012. Human prefrontal cortex: evolution, development, and pathology. *Prog Brain Res*. 195:191–218.
- Tournier JD, Hughes E, Tusor N, Sotiropoulos SN, Jbabdi S, Andersson J, Rueckert D, Edwards AD, Hajnal JV. 2015. Data-driven optimisation of multi-shell HARDI. In: *Proceedings of the 23rd Annual Meeting of ISMRM*. Toronto, Canada, p. 2897.
- Tournier JD, Smith R, Raffelt D, Tabbara R, Dhollander T, Pietsch M, Christiaens D, Jeurissen B, Yeh CH, Connelly A. 2019. MRtrix3: a fast, flexible and open software framework for medical image processing and visualisation. *Neuroimage*. 202:116137.
- van den Heuvel MP, Kersbergen KJ, de Reus MA, Keunen K, Kahn RS, Groenendaal F, de Vries LS, Benders MJNL. 2015. The neonatal connectome during preterm brain development. *Cereb Cortex*. 25:3000–3013.
- Veraart J, Novikov DS, Christiaens D, Ades-aron B, Sijbers J, Fieremans E. 2016. Denoising of diffusion MRI using random matrix theory. *Neuroimage*. 142:394–406.
- von Economo C, Koskinas G. 1925. *Die Cytoarchitektonik der Hirnrinde des erwachsenen Menschen*. Berlin: Springer.
- Whitaker KJ, Vértes PE, Romero-Garcia R, Váša F, Moutoussis M, Prabhu G, Weiskopf N, Callaghan MF, Wagstyl K, Rittman T et al. 2016. Adolescence is associated with genomically patterned consolidation of the hubs of the human brain connectome. *Proc Natl Acad Sci U S A*. 113:9105–9110.
- Yee Y, Fernandes DJ, French L, Ellegood J, Cahill LS, Vousden DA, Spencer Noakes L, Scholz J, van Eede MC, Nieman BJ et al. 2018. Structural covariance of brain region volumes is associated with both structural connectivity and transcriptomic similarity. *Neuroimage*. 179:357–372.
- Zhang H, Schneider T, Wheeler-Kingshott CA, Alexander DC. 2012. NODDI: practical in vivo neurite orientation dispersion and density imaging of the human brain. *Neuroimage*. 61:1000–1016.
- Zhao T, Xu Y, He Y. 2019. Graph theoretical modeling of baby brain networks. *Neuroimage*. 185:711–727.
- Zielinski BA, Gennatas ED, Zhou J, Seeley WW. 2010. Network-level structural covariance in the developing brain. *Proc Natl Acad Sci USA*. 107:18191–18196.
- Zuo Z, Ran S, Wang Y, Li C, Han Q, Tang Q, Qu W, Li H. 2018. Altered structural covariance among the dorsolateral prefrontal cortex and amygdala in treatment-Naïve patients with major depressive disorder. *Front Psych*. 9:323.